Technical University of Denmark

DTU

# Improvement of Dynamic Performance of Hybrid Gas Bearings via Adjustable Lubrication

**Pierart Vásquez, Fabián Gonzalo; Santos, Ilmar**

Link back to DTU Orbit

DTU Library
Technical Information Center of Denmark

# Improvement of Dynamic Performance of Hybrid Gas Bearings via Adjustable Lubrication
# Amélioration des Performances Dynamiques de Paliers Hybrides à Gaz par Lubrification Ajustable

F.G. Pierart and I.F. Santos

*Department of Mechanical Engineering, Technical University of Denmark, 2800 lyngby, Denmark.*

In modern turbo-machinery gas journal bearings have been increasingly adopted, because they can operate at higher speed than most bearing designs. The main disadvantage of gas bearings is their low dynamic stability range. One solution to improve this and their performance is to combine the aerodynamic effect with the addition of external pressurization in a hybrid gas bearing.

This study uses a mathematical model for hybrid lubrication of a compressible fluid film journal bearing with adjustable control of the external pressure, developed previously in [12]. The model is based on a compressible form of Reynolds Equation. To include the effect of the injection, an extra term is added to the Reynolds Equation, considering the fully developed Hagen-Poeiseuille flow in the injection pipeline.

In order to verify this assumption, a Computational Fluid Dynamics (CFD) model is developed and the pressure and velocity fields in the injection nozzle are compared. The simplified theoretical model has been validated against the CFD results and experimentally using a test rig. The test rig consists of a flexible rotor supported by a ball bearing and a controllable hybrid gas bearing.

The results show that the level of pressure has a strong influence in the dynamic behavior of the system, and with the correct level of pressure and different pressurization strategies it is possible to improve the dynamic performance of the system.

Dans les turbomachines modernes, les paliers lisses gaz sont de plus en plus choisis, parce qu'ils peuvent fonctionner à une vitesse plus élevée que la plupart des autres conceptions de palier. Le principal inconvénient des paliers à gaz est leurs faibles performances dynamiques de stabilité. Une solution pour les améliorer est d'associer l'effet aérodynamique avec une source externe de pression dans un palier à gaz hybride.

Cette étude présente un modèle mathématique pour la lubrification hybride d'un palier avec un fluide compressible et une commande de réglage de la pression externe. Le modèle est basé sur une forme compressible de Reynolds équation. Pour comprendre l'effet de l'injection, un terme supplémentaire est ajouté à l'équation de Reynolds, compte tenu du flux Hagen-Poiseuille entièrement développé dans circuit d'injection.

Afin de vérifier cette hypothèse, un modèle CFD est développé et les champs de pression et de vitesses dans la buse d'injection sont comparés. Le modèle théorique a été validé expérimentalement en utilisant un banc d'essai. Le dispositif d'essai se compose d'un rotor flexible supporté par un roulement à billes et un palier à gaz hybride contrôlable.

Les résultats montrent que le niveau de pression a une forte influence sur le comportement dynamique du système et, avec le bon niveau de pression, il est possible d'améliorer les performances dynamiques du système.

*12th EDF/Pprime Workshop:*
*"Solutions for performance improvement and friction reduction of journal and thrust bearings"*

Futuroscope, September 17 & 18, 2013

# 1    Introduction

Gas journal bearings have been increasingly adopted in modern turbo-machinery, since they exhibit numerous indisputable advantages. They can operate at higher speed than most bearing designs, reaching speeds as high as 1 Mrpm [1], almost without noise or heat generation. In most cases, as in this work, the gas used is air, which is cheap, abundant and clean. Furthermore, it is shown that gas bearings have great efficiency [2].

Currently, gas bearings are used in air management systems for aircraft, in micro-gas turbines as independent power generators, in turbocompressors, micromachinery tools, and in many other applications. However these bearing are prone to instability under certain operating conditions [3].

The stability of gas-lubricated hydrodynamic bearings has been studied since the 1960s. The first studies were focused on investigating the threshold mass and the threshold speed of rotors supported by hydrodynamic gas bearings, using for example Galerkin's method [4-5].

Additional investigations to improve characteristics of gas bearings were carried out. Vleugels et al. [1] presented a model to predict the steady-state behavior of a foil bearing, showing that a foil gas bearing is more stable than a rigid hydrodynamic journal bearing with similar geometry. Lund [6-7] carried out two studies in which the stiffness and damping coefficients were calculated to examine the whirl instabilities of 3-lobe tilting pad and externally pressurized gas bearings.

Subsequent studies [8–10] investigated externally pressurized air bearings numerically by various mathematical approaches for various configurations of compensation of pressurized air.

Experimental investigation of hydrostatic gas journal bearings was also performed by Leonard and Rowe [11], in which the dynamic force coefficients and the mechanism of the whirling were investigated and the theoretical predictions of the onset of instability by mathematical correlations were shown to be in good match with experiments.

Morosi & Santos [12] presented a theoretical model based in the solution of the modified Reynolds equation (MRE), to predict the dynamic behavior of an active hybrid gas bearing. The present work is focused on this kind of gas bearing, because it additionally improves the start-up and shut-down properties, the carrying capacity, and more important, it allows adjustments of the external injection pressure.

For incompressible fluids the theoretical model, based on the Modified Reynolds Equation for active lubrication, is able to capture the pressure profiles and furthermore the controllable fluid forces quite accurately for a static condition [13]. For compressible fluids the extension of the Modified Reynolds Equation has to be carefully validated via comparison to CFD simulations. In this framework the main objective of this study is to validate the simplified model based on the Modified Reynolds Equation [12]; take advantage of such a simplified model to accurately predict the stiffness and damping characteristics of hybrid gas bearings using different pressurization strategies; and hence improve the stability and performance of the hybrid gas bearings.

# 2    Test Facilities

The mechanical system used for the experimental work is shown in Fig.1. The system consists of a rotor supported by two types of bearings, one ball bearing (3) and one gas bearing (5) and it has a disc attached to its end (6). The rotor is driven by a gas turbine (1) and the torque from the turbine is transmitted to the shaft (4) with the aid of flexible couplings (2). Two inductive proximity sensors are fixed to the holder around the disc (8) and an incremental encoder is mounted at the end of the shaft just before the flexible couplings.
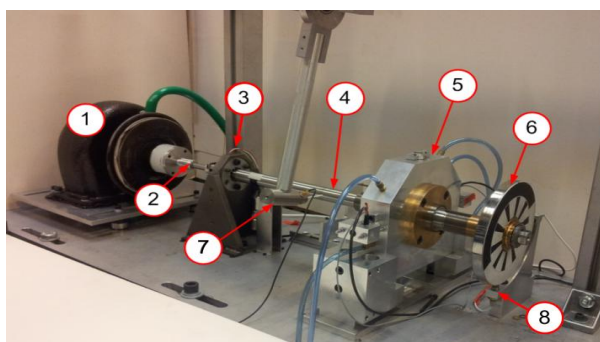


***Fig 1 – Overview of the experimental test rig [12].***

## 2.1 Rotor and disc

The main dimensions of the flexible shaft and the disc of the rotor-bearing test rig are shown in Fig. 2. The total length of the shaft is 500 mm, with the main diameters of 40, 30 and 22 mm. The shaft is made of stainless steel type 314, with a total weight of approximately 2 kg. The disc is made of steel, its outer diameter is 140 mm and the total weight is 1.5 kg.
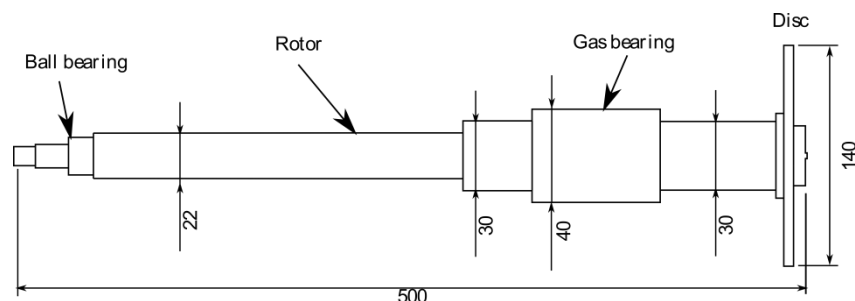


***Fig 2 - Schematic view of the mechanical system and principal dimensions in mm.***

## 2.2 Hybrid gas bearing

The gas journal bearing consist of four main parts, see Figs. 3-4: a bronze sleeve (1), an aluminum housing (2), adjustable mounts (5) and a sub-plate (4).
The injection of air takes place through four orifices drilled in the gas bearing sleeve. The orifices have a diameter of 2 *mm* and they are equally distributed, every 90°, as is shown in Fig.4.
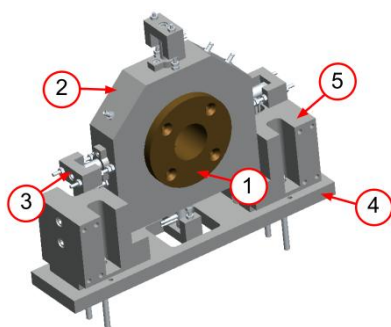


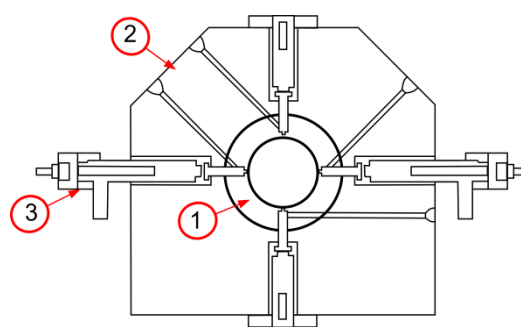***Fig 3 – Isometric view of assembled gas journal bearing [12].***



***Fig 4 – Gas journal bearing cross section and electro-mechanical subsystems built by piezoactuators [12].***

### 2.2.1 Gas journal bearing injection system

The gas journal bearing injection system is composed of four independent electro-mechanical subsystems, see Fig. 4. The electro-mechanical subsystems are built by piezoactuators which allow pressure-flow control of the air injection. With the goal of testing the principle only two piezoactuators are initially mounted in the test rig. One of these injection subsystems is presented in details in Fig. 5. The piezoactuator (1) push the pin (2) in the direction of the gas bearing center. The piezoactuator is not capable to pull the pin back; therefore a Belleville washer is implemented (3). An O-ring seal (4) is used to ensure that the pressurized air escapes only through the orifice.

Each of the injection orifices is fed by pressurized air from an internal compressed air network. The supply pressure is approximately 7.5 bar (gauge). The supply pressure is measured by a pressure indicator (1) and it can be adjusted by gently closing/opening the ball valve (2), see Fig. 6.
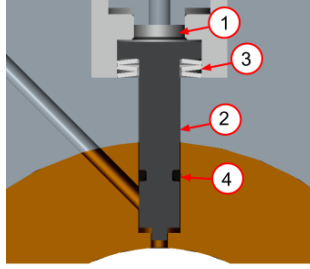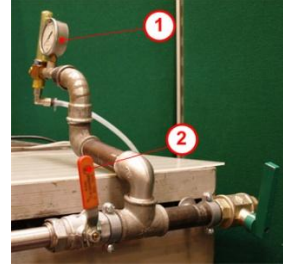
**Fig 5 – Details of injection system [12].**



**Fig 6 – Pressure indicator (1) and ball valve (2) for pressurized air supply.**

## 3 Theoretical model

In this section the theoretical model (MRE) proposed in [12] it is explained. A finite element (FE) approach has been followed. The rotor is modeled as a flexible shaft, where only lateral movement is considered, structural damping is neglected. The choice of finite elements of the shaft is shown in Fig. 7.
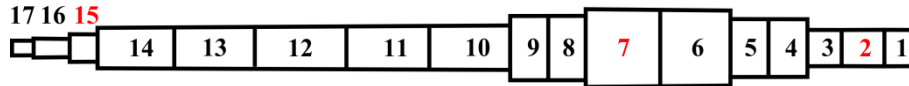


**Fig 7 – Shaft discretization for the FEM model.**

The equation of motion for the rotor can be written as:

$$\left(M_T^S + M_R^S\right)\ddot{q} + D^S \dot{q} + K^S q = Q^S, \tag{1}$$

where the superscript $^S$ refers to the shaft, $M_T^S$ is the mass matrix contribution of the translational degrees of freedom (dofs) and $M_R^S$ of the rotational dofs. The damping matrix $D^S = -\Omega G^S$ is given by the gyroscopic effect and $K^S$ the bending stiffness. The angular velocity of the shaft is $\Omega$.
The disc is considered to be a rigid body, and the equation of motion can be written as:

$$M^d \ddot{q} - \Omega G^d \dot{q} = Q^d, \tag{2}$$

where the superscript $^d$ refers to the disc. The bearings are modeled as linear forcing elements acting on the rotor and the housing as clamps, and the equation of motion can be written as:

$$Q^b = -D^b \dot{q} - K^b q \tag{3}$$

To obtain the global set of equations of motion, the superposition principle is used. The shaft is discretized using 18 nodes (17 shaft elements) as shown in Fig. 7. The two bearings and the disc are placed in nodes 15, 7 and 2 respectively. The global finite element model is of order 17, built by global mass, stiffness, damping and gyroscopic matrices and it is given by:

$$M^g \ddot{q} + D^g \dot{q} + K^g q = Q^g \tag{4}$$

### 3.1 Hybrid gas bearing

To obtain the dynamics coefficients $D^b$ and $K^b$ used in Eq. (3) for the hybrid gas bearing, the Reynolds equation is solved according to the procedure described by Lund and Thomsen [14]. The compressible Reynolds equation is shown in Eq. (5).

*12th EDF/Pprime Workshop:*
*"Solutions for performance improvement and friction reduction of journal and thrust bearings"*

*Futuroscope, September 17 & 18, 2013*

$$\frac{\delta}{\delta x}\left(\frac{\rho h^3}{\mu}\frac{\delta p}{\delta x}\right) + \frac{\delta}{\delta y}\left(\frac{\rho h^3}{\mu}\frac{\delta p}{\delta y}\right) = 6U\frac{\delta}{\delta x}(\rho h) + 12\frac{\delta \rho h}{\delta t} \qquad (5)$$

To relate the density with the other state variables, the ideal gas law is used.

$$\rho = \frac{pM}{RT} \qquad (6)$$

Where *M* is the molar mass, *R* the universal gas constant and *T* the gas temperature. Considering also the assumption that the gas bearing work in near-isothermal condition [14], only the pressure *p* is not a constant and using Eq. (6) in Eq. (5), it can be written in a general form:

$$\frac{\delta}{\delta x}\left(\frac{ph^3}{\mu}\frac{\delta p}{\delta x}\right) + \frac{\delta}{\delta y}\left(\frac{ph^3}{\mu}\frac{\delta p}{\delta y}\right) = 6U\frac{\delta}{\delta x}(ph) + 12\frac{\delta ph}{\delta t} \qquad (7)$$

To include the effect of an external injection of air into the Reynolds equation, a simple modification to the standard reduction of the Navier-Stokes equations is introduced. For the external radial injection, a velocity profile is defined in the domain comprised between the supply chamber and the bearing, according to the Hagen-Poeiseuille formula shown in Eq. (8). This procedure has, however, some limiting assumptions. It is assumed that the radial injection flow is laminar and fully developed; moreover the flow is considered incompressible.

$$V_{inj}(y,z,t) = -\frac{1}{4\mu}\frac{\delta p}{\delta x}\left[\frac{d_0^{\,2}}{4} - (y - y_1)^2 - (z - z_1)^2\right] \qquad (8)$$

Adding this extra term to the Reynolds equation defined in Eq. (7), the modified Reynolds equation can be written as:

$$\frac{\delta}{\delta x}\left(\frac{ph^3}{\mu}\frac{\delta p}{\delta x}\right) + \frac{\delta}{\delta y}\left(\frac{ph^3}{\mu}\frac{\delta p}{\delta y}\right) = 6U\frac{\delta}{\delta x}(ph) + 12\frac{\delta ph}{\delta t} + 12\frac{p}{\mu}V_{inj} \quad (9)$$

Note that the extra term $12\frac{p}{\mu}V_{inj}$ is only to be included in orifice areas, whereas it is zero elsewhere.

The film thickness function *h* depends on the position of the center of the shaft according to Eq. (10):

$$h = C + e_x\cos(\theta) + e_y\sin(\theta), \qquad (10)$$

where *C* depends on the geometry, which in this case is a cylindrical geometry, giving $C = R_e - R_i$.

In order to calculate the stiffness and damping coefficients a harmonic perturbation method is used. The movement of the rotor at rotational speed $\omega$ around an equilibrium position with small harmonic amplitude is defined as:

$$e_x = e_{x0} + \Delta e_x e^{i\omega t} \qquad (11)$$

Using Eq. (11) in the film thickness function Eq. (10) and pressure fields leads to:

$$p = p_0 + (\Delta e_x p_x + \Delta e_y p_y)e^{i\omega t} \qquad (12)$$

$$h = C + e_{x0}\cos(\theta) + e_{y0}\sin(\theta) + (\Delta e_x\cos(\theta) + \Delta e_y\sin(\theta))e^{i\omega t} \quad (13)$$

Separating steady state (zeroth order) and perturbed (first order) terms and inserting in to Eq. (9), and thereby neglecting higher order terms, the zeroth and first order equation are:

-Zeroth order

$$\frac{\delta}{\delta x}\left(\frac{p_0 h_0^3}{\mu}\frac{\delta p_0}{\delta x}\right) + \frac{\delta}{\delta y}\left(\frac{p_0 h_0^3}{\mu}\frac{\delta p_0}{\delta y}\right) = 6U\frac{\delta}{\delta x}(p_0 h_0) \qquad (14)$$

-First order

$$\frac{\delta}{\delta x}\left(\frac{p_0 h_0^3}{\mu}\frac{\delta p_X}{\delta x} + \frac{p_X h_0^3}{\mu}\frac{\delta p_0}{\delta x}\right) + \frac{\delta}{\delta y}\left(\frac{p_0 h_0^3}{\mu}\frac{\delta p_X}{\delta y} + \frac{p_X h_0^3}{\mu}\frac{\delta p_0}{\delta y}\right) - 6U\frac{\delta}{\delta x}(p_0 h_0) - \ldots$$

$$\ldots - 12i\omega(p_X h_0) = -\frac{\delta}{\delta x}\left(3\frac{p_0 h_0^2}{\mu}\frac{\delta p_0}{\delta x}\cos(\theta)\right) - \frac{\delta}{\delta y}\left(3\frac{p_0 h_0^2}{\mu}\frac{\delta p_0}{\delta y}\cos(\theta)\right) + \ldots$$

$$\ldots + 6U\frac{\delta}{\delta x}(p_0\cos(\theta)) + 12i\omega(p_0\cos(\theta)) \qquad (15)$$

The pressure distribution in the bearing is continuous in the circumferential coordinate and equal to the atmospheric value at the bearing sides. The boundary conditions for the steady-state and the perturbation Eq. (15) are defined by:

$$p_0(x,0) = p_0(x,L) = p_{atm}$$
$$p_0(0,y) = p_0(2\pi R, y) \qquad (16)$$
$$\frac{\delta p_0(0,y)}{\delta x} = \frac{\delta p_0(2\pi R, y)}{\delta x}$$

For a given operation condition and eccentricity, the nonlinear partial differential equation (14) is solved using a finite difference approximation on a discretized domain. The zeroth order pressure field is integrated over the bearing surface, which in turn imposes vertical and horizontal static hydrodynamic reaction forces:

$$F_X = \int_0^L \int_0^{2\pi} (p_0 - p_{atm})\cos(\theta)Rd\theta dy \qquad (17)$$

$$F_Z = \int_0^L \int_0^{2\pi} (p_0 - p_{atm})\sin(\theta)Rd\theta dy \qquad (18)$$

The solution of the first-order perturbation equations (for the perturbed pressures) is straightforward. Given a zeroth-order field $p_0$ they are solved via a finite difference scheme and subsequently integrated over the bearing surface to determinate the stiffness and damping coefficients:

$$K + i\omega D = \int_0^L \int_0^{2\pi} \begin{bmatrix} p_X\cos\theta & p_X\sin\theta \\ p_Y\cos\theta & p_Y\sin\theta \end{bmatrix} Rd\theta dy \qquad (19)$$

## 3.2    CFD analysis

In order to verify the assumption made in Eq. (9), a computational fluid dynamics (CFD) model is developed.

### 3.2.1    Solution procedure

The governing equations have been solved for steady state conditions using the open source CFD code OpenFOAM-2.0.1 with the rhoSimplecFoam solver. This solver is based on the SIMPLE (Semi Implicit Pressure Linked Equation) algorithm.

The numerical schemes used in the rhoSimpleFoam solver in the present study are listed in Table 1.

| Gradient | Gauss linear | | | | |
|---|---|---|---|---|---|
| Divergence | Gauss upwind | | | | |
| Laplacian | Gauss linear corrected | | | | |
| Under-relaxation factors | | | | | |
| p | rho | U | h | k | epsilon |
| 0.1 | 0.7 | 0.9 | 0.7 | 0.5 | 0.7 |

***Tab 1 – Parameters used in CFD code.***

The convergence criteria for all cases are set to residual values of $10^{-4}$ for the pressure field and $10^{-6}$ for other flow field variables.

### 3.2.2   Geometry, computational domain and meshing

The simulation of the whole injection system, which consists of four injection orifices and a rotating shaft, requires significant CPU resources. Therefore, the CFD model is simplified, so that only a part of one injection chamber is modeled. This is illustrated in Fig.8.
The surface of the rotor is modeled as a straight surface because of the relative high dimensions of the rotor compare with the injector. Also only a half of the geometry is considered and thereby the symmetry is exploited. The computational domain is divided into 7 patches: inlet, outlet, symmetry plane, cyc1, cyc2 (cyclic boundaries), fixed wall and moving wall. See Fig. 9.
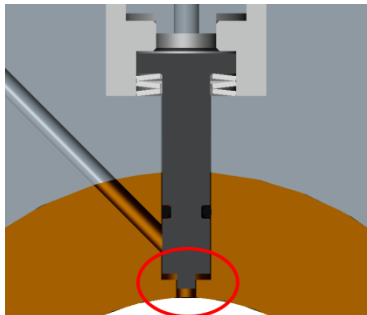


***Fig. 8 – Part of the subsystem used in CFD model.***
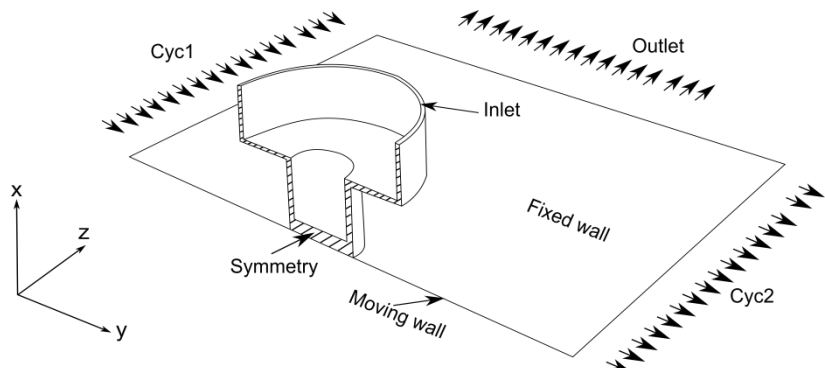


***Fig 9 - Isometric view of the CFD model.***

To create the mesh the *blockMesh* tool is used, because of the relatively simple geometry. The principle behind *blockMesh* is to decompose the domain geometry into a set of one or more three dimensional, hexahedral blocks. The mesh used in this work has 145600 cells, a schematic view is shown in Fig. 10.



***Fig 10 – Schematic view of the CFD model mesh.***

Air is used as lubricant; pressure, temperature and density are related by ideal gas law.

*12<sup>th</sup> EDF/Pprime Workshop:*
*"Solutions for performance improvement and friction reduction of journal and thrust bearings"*

*Futuroscope, September 17 & 18, 2013*

### 3.2.3    Boundary conditions

The boundary conditions are defined as follows:

Inlet:
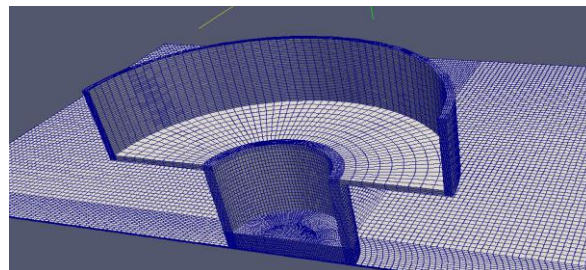- Fixed pressure: (800.5 kPa, 600 kPa and 400 kPa)
- Fixed temperature: 288 K

Outlet:
- Atmospheric pressure: 100 kPa
- Fixed temperature: 290 K

Moving wall:
- The lower surface has a linear velocity in the y direction.

For the y direction (radial) a periodic or cyclic condition is imposed.


## 4    Results and Analysis

### 4.1    CFD results

The simplified theoretical model based on MRE for compressible fluids present by Morosi & Santos [12] is compared to the CFD model, focusing on the injection zone. It is important to mention that the CFD model is limited to a staedy state and the dynamic behaivor of the rotor-bearing system cannot be observed in the CFD model. For this reason, the gap between rotor and bearing surfaces is constant in the CFD model, whereas the gap for the MRE is not constant and varies according to the equation (13), depending on the rotor angular velocity.

In order to evaluated the simplifications made in the MRE model and taking into account the limitation of a steady state for the CFD model, pressure and velocity fields in the injection zone (see Fig. 11) are compared.



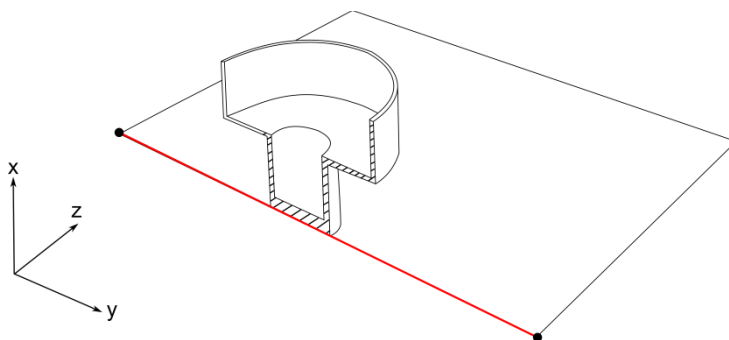***Fig 11 – Line where the pressure and velocity profile are compared.***


In Figure 12 the pressure profile is illustrated. The results are obtained using MRE, equation (9), as well as the CFD model. A comparison between MRE and CFD reveals that the influence of rotor angular velocity on the pressure profile is negligible; this is consistent according to the simplification of a steady state model.
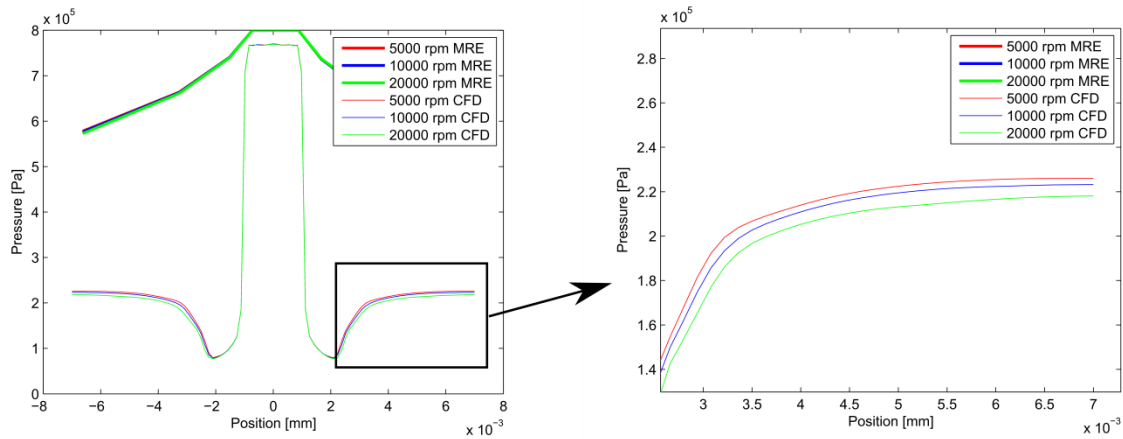
*12<sup>th</sup> EDF/Pprime Workshop:*
*"Solutions for performance improvement and friction reduction of journal and thrust bearings"*

*Futuroscope, September 17 & 18, 2013*

***Fig 12 – Comparison of pressure profile for CFD and theoretical model, injection pressure 8 bar.***

In Figure 13 the pressure and the resultant velocity are illustrated, for a rotor angular velocity of 5000 rpm (low angular velocity). The results using MRE, equation (9), and CFD model are compared.
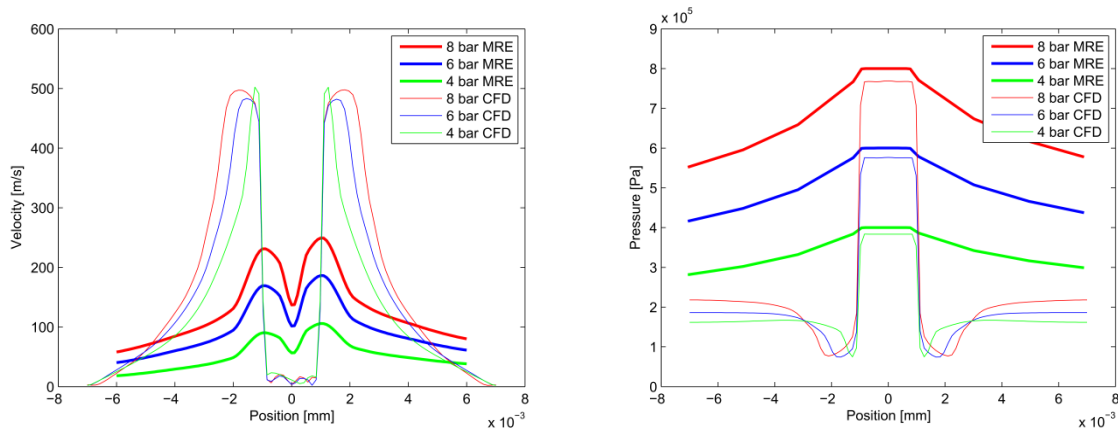


***Fig 13 – Comparison of velocity and pressure profile, for CFD and theoretical model, rotor angular velocity 5000 rpm.***

The difference between the CFD model and the theoretical model (MRE) as shown in Fig. 13 are produced by the effect of the change in the volume when the fluid flows from the injector region into the bearing gap. This change of volume produces a rapid increment in the velocity and decrement in the pressure. This also leads to a decrease in temperature; this effect is more clear in the Fig. 14.

Fig. 14 illustrates the pressure, temperature, velocity and Mach number distributions obtained via CFD modeling, for a rotor angular velocity equal to 5000 rpm (low angular velocity) and an injection pressure of 8 bar. A cut plane is used in the middle section of the gap between the rotor and bearing surface.
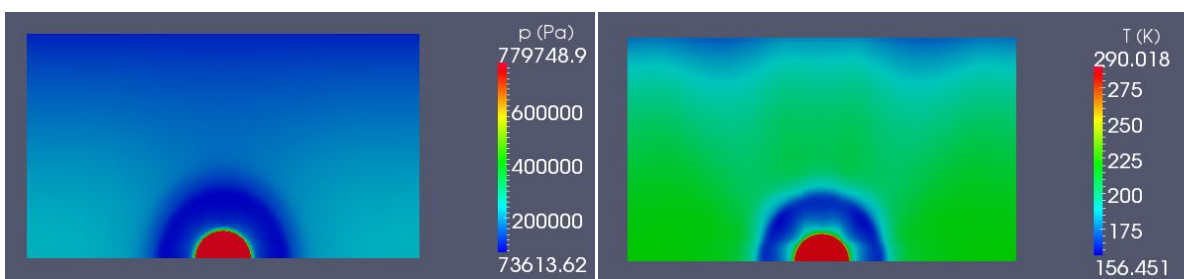
*Fig 14 – Pressure temperature velocity and Mach number distribution, CFD model.*

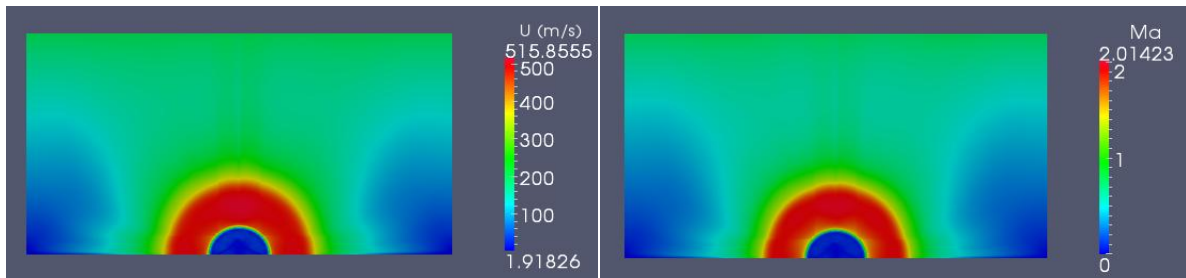The theoretical model (MRE) assumes an incompressible and isothermal behavior for the flow in the injection area. The results of the CFD model (Fig. 14) show that these assumptions are not correct, and these effects should be considered.

## 4.2 Comparison between CFD and theoretical model based in MRE

In order to evaluate the difference between the CFD and MRE models, the force produced by the air in the bearing and injection section is studied. The force is calculated for only a quarter part of the bearing, taking advantage of the symmetry. These results are shown in Table 2.

| 5000 rpm | 4 bar | 6 bar | 8 bar |
|---|---|---|---|
| CFD model | 39.8 N | 46.2 N | 53.7 N |
| Theoretical model | 55.22 N | 79.40 N | 104.04 N |
| Absolute error | 27.8% | 41.8% | 48.3% |

| 10000 rpm | 4 bar | 6 bar | 8 bar |
|---|---|---|---|
| CFD model | 39.4 N | 46.0 N | 53.5 N |
| Theoretical model | 55.24 N | 79.42 N | 104.06 N |
| Absolute error | 28.6% | 42.1% | 48.5% |

*Tab 2 – Comparison of the force in the bearing and injection section, between the CFD and theoretical model.*

It is important to mention, that the error in calculating the force will be much smaller if the region outside of the orifice zone is taking into account.

## 4.3 Experimental results

In Figs. 15 and Tables 3-4, natural frequencies and damping factors as a function of the rotor angular velocity and the injection pressure in the gas bearing are illustrated. The results using the MRE equation (9) are compared with the experimental results.
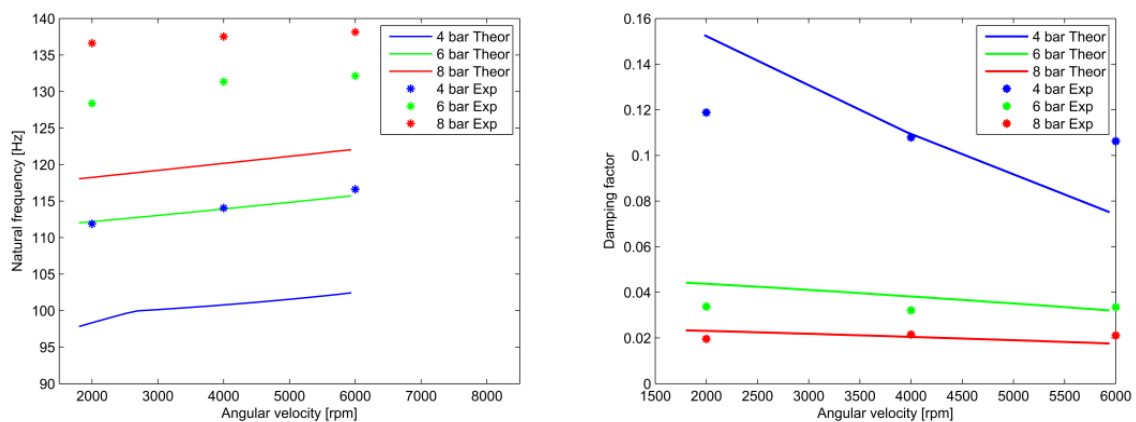


*Fig 15 – Natural frequencies and damping factor comparison theoretical model (MRE) and experimental results.*

*12<sup>th</sup> EDF/Pprime Workshop:*
*"Solutions for performance improvement and friction reduction of journal and thrust bearings"*

*Futuroscope, September 17 & 18, 2013*

|  | Theoretical (Hz) | Experimental (Hz) | Absolute error |
|---|---|---|---|
| 4 bar, 2000 rpm | 96.8 | 111.9 | 13.4% |
| 6 bar, 2000 rpm | 111.4 | 128.4 | 13.2 % |
| 8 bar, 2000 rpm | 118.7 | 136.6 | 13.1 % |
| 4 bar, 4000 rpm | 97.9 | 114.0 | 14.3% |
| 6 bar, 4000 rpm | 112.7 | 131.3 | 14.1 % |
| 8 bar, 4000 rpm | 120.3 | 137.5 | 12.7 % |
| 4 bar, 6000 rpm | 100.0 | 116.6 | 14.2% |
| 6 bar, 6000 rpm | 114.4 | 132.1 | 13.3 % |
| 8 bar, 6000 rpm | 122.7 | 138.1 | 12.7% |

***Tab 3 – Comparison of natural frequencies, between the theoretical model (MRE) and experimental results.***

In Table 3 it is possible to see that the error is almost constant around 13% for natural frequencies.

| Damping Factor | Theoretical | Experimental (Hz) | Absolute error |
|---|---|---|---|
| 4 bar, 2000 rpm | 0.15 | 0.12 | 20.0% |
| 6 bar, 2000 rpm | 0.07 | 0.03 | 57.1 % |
| 8 bar, 2000 rpm | 0.04 | 0.02 | 50.0 % |
| 4 bar, 4000 rpm | 0.11 | 0.11 | 0.0% |
| 6 bar, 4000 rpm | 0.06 | 0.03 | 50.0 % |
| 8 bar, 4000 rpm | 0.04 | 0.02 | 50.0 % |
| 4 bar, 6000 rpm | 0.08 | 0.11 | 37.5% |
| 6 bar, 6000 rpm | 0.05 | 0.03 | 40.0 % |
| 8 bar, 6000 rpm | 0.03 | 0.02 | 33.3 % |

***Tab 4 – Comparison of damping factors between the theoretical model (MRE) and experimental results.***

## 4.4    Effects of the pressure in the stability range

The theoretical model based on the MRE model is used to simulate the dynamic behavior of the rotor-bearing system. The effects of the different injection strategies are studied.

Fig. 16 illustrates the theoretical behavior of the equilibrium position of the rotor-bearing system illustrated in Fig.1 as a function of rotor angular velocity [4000 rpm to 20000 rpm] considering different injection strategies: a) without injection; b) injection using 4 orifices with equal pressure of 4 bar; c) injection using 2 orifices placed vertically and opposed to each other with equal pressure of 4 bar; d) injection using 4 orifices with equal pressure of 8 bar ; e) injection using 2 orifices placed vertically and opposed to each other with equal pressure of 8 bar.
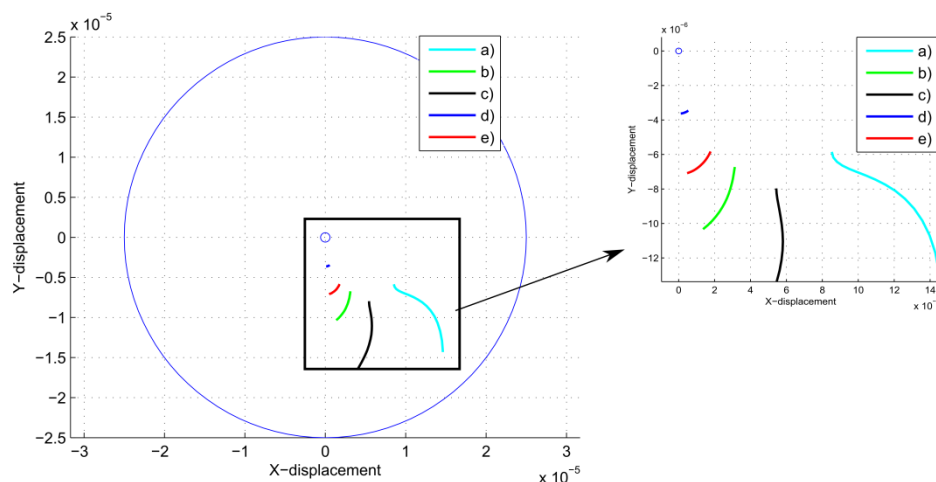


***Fig 16 – Equilibrium position as function of rotor angular velocity for the five configurations: a) without injection; b) injection using 4 orifices with equal pressure of 4 bar; c) injection using 2 orifices placed vertically and opposed to each other with equal pressure of 4 bar; d) injection using 4 orifices with equal pressure of 8 bar; e) injection using 2 orifices placed vertically and opposed to each other with equal pressure of 8 bar.***

*12<sup>th</sup> EDF/Pprime Workshop:*
*"Solutions for performance improvement and friction reduction of journal and thrust bearings"*

*Futuroscope, September 17 & 18, 2013*

From results shown in Fig. 16, it can be noticed that for a higher injection pressure (red and blue lines) the equilibrium position is closer to the center of the bearing and hence more prone to instability. The use of pressurization in both orthogonal directions also produces an equilibrium position closer to center compared with the use of pressurization in one single direction.

For the same pressure strategies from a) to e), stiffness and damping coefficients for the gas bearing are illustrated in Fig 17. The load applied to the bearing corresponds to the shaft-disc weight (4 kg), and the rotor angular velocity varies from 4000 rpm to 20000 rpm.
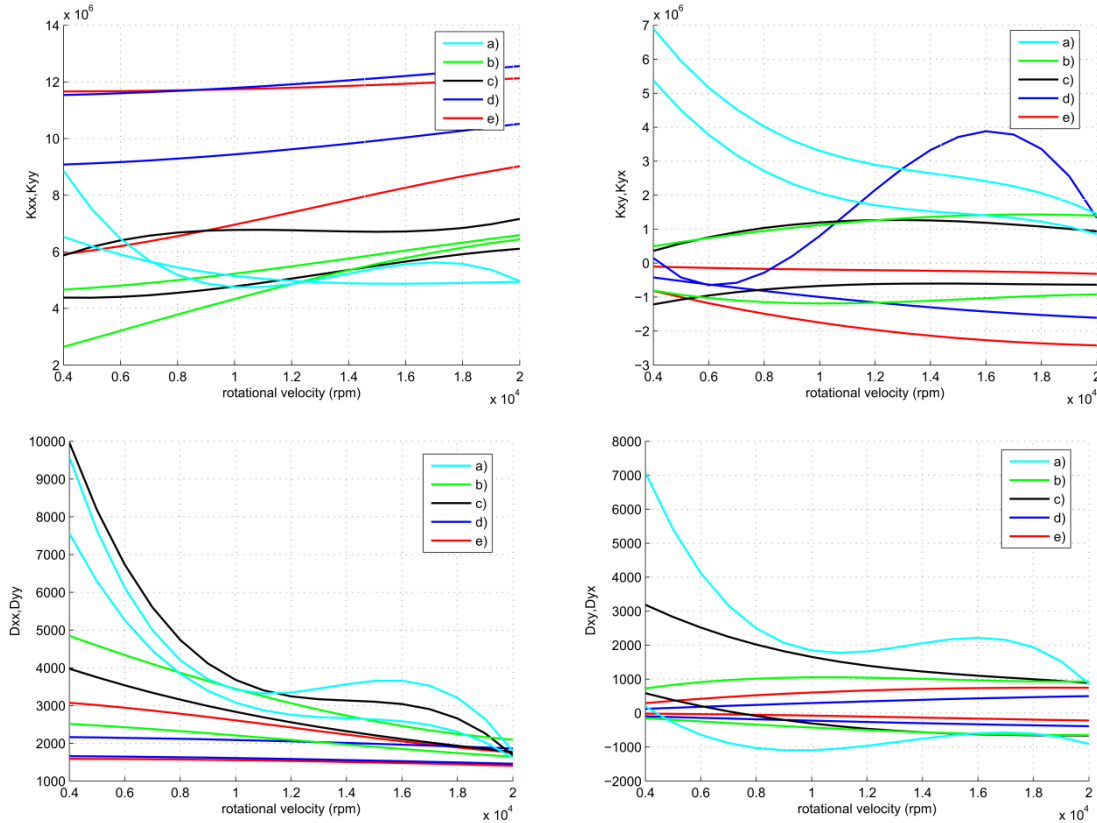


*Fig 17 – Stiffness and damping coefficients for the five configurations: a) without injection; b) injection using 4 orifices with equal pressure of 4 bar; c) injection using 2 orifices placed vertically and opposed to each other with equal pressure of 4 bar; d) injection using 4 orifices with equal pressure of 8 bar; e) injection using 2 orifices placed vertically and opposed to each other with equal pressure of 8 bar.*

In Fig.17 it is possible to see that direct stiffness coefficients increase for higher level of injection pressure and the use of injection pressurization in one single direction produces larger differences between $K_{xx}$ and $K_{yy}$ than when pressurizing the bearing in both orthogonal directions. Looking at the cross-coupled stiffness terms, one observes that the use of injection with 4 bar tends to assume a more clear asymmetric behavior than when a pressure of 8 bar is used. In relation with the use of pressurization in one or two directions it is not possible to see a clear effect in the cross-coupled stiffness terms.

For the direct damping coefficients, it is possible to see a similar behavior to the direct stiffness coefficients, where the use of injection pressurization in one single direction produces larger differences between $D_{xx}$ and $D_{yy}$ than when pressurizing the bearing in both orthogonal directions. Here the direct damping coefficients decrease for higher levels of pressure. In relation to the cross-coupled damping coefficients all configurations tend to an asymmetric behavior.

In Figs. 18-19 the real and imaginary part of the eigenvalues of the system are plotted as function of the angular velocity [5200 rpm to 20000 rpm] for the configurations a) to e).

*12th EDF/Pprime Workshop:*
*"Solutions for performance improvement and friction reduction of journal and thrust bearings"*
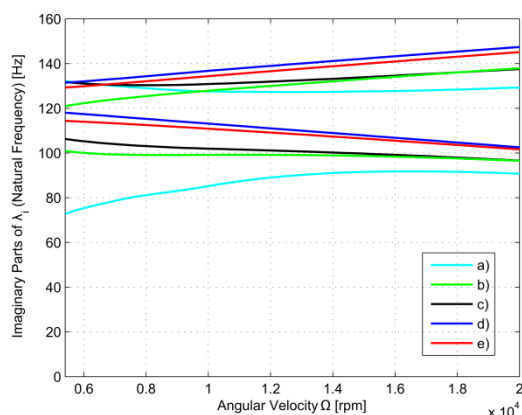
*Futuroscope, September 17 & 18, 2013*

*Fig 18 – Campbell diagram for the five configurations a) without injection; b) injection using 4 orifices with equal pressure of 4 bar; c) injection using 2 orifices placed vertically and opposed to each other with equal pressure of 4 bar; d) injection using 4 orifices with equal pressure of 8 bar; e) injection using 2 orifices placed vertically and opposed to each other with equal pressure of 8 bar.*
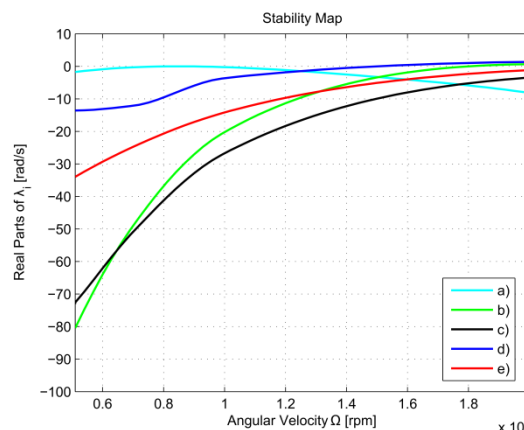
*Fig 19 – Stability map for the five configurations a) without injection; b) injection using 4 orifices with equal pressure of 4 bar; c) injection using 2 orifices placed vertically and opposed to each other with equal pressure of 4 bar; d) injection using 4 orifices with equal pressure of 8 bar; e) injection using 2 orifices placed vertically and opposed to each other with equal pressure of 8 bar.*

The analysis of the imaginary part of the eigenvalues shows that the natural frequencies are higher for a higher level of injection pressure. This behavior is consistent with the results shown in Fig. 17, where the stiffness coefficients present the same behavior. In relation to the use of two or four injectors, it is not possible to see a clear difference between the two strategies in the natural frequencies.

The real part of the eigenvalues shows the stability threshold of the rotor-bearing system, i.e. when the real part of one of the eigenvalues becomes positive the system becomes unstable. Comparing the hydrostatic results (no injector) with the results for the hybrid operation cases, it is noticed that the rotor-bearing system operating under hybrid lubrication conditions has higher stability threshold. It is also possible to see that the use of only two injectors produce higher stability threshold. Such a claim is consistent with the behavior of the damping and stiffness coefficients and the equilibrium position plot presented in Figs. 16-17. In table 5 the stability threshold for the five strategies of analyzed pressurization is illustrated.

| | a) | b) | c) | d) | e) |
|---|---|---|---|---|---|
| Stability threshold | 8400 (rpm) | 20000 (rpm) | 28000 (rpm) | 13000 (rpm) | 22000 (rpm) |

*Tab 5 – Threshold speed for five pressurization strategies a) without injection; b) injection using 4 orifices with equal pressure of 4 bar; c) injection using 2 orifices placed vertically and opposed to each other with equal pressure of 4 bar; d) injection using 4 orifices with equal pressure of 8 bar; e) injection using 2 orifices placed vertically and opposed to each other with equal pressure of 8 bar.*

## 5    Conclusions

The simplified theoretical model based on MRE for compressible fluids present by Morosi & Santos [12] is compared to a CFD model, focusing on the injection zone. While no significant discrepancies in terms of pressure distribution can be detected for uncompressible fluid [13], it is not the case for compressible fluid. The results presented in the paper show some discrepancies between MRE and CFD. The simplified model based on MRE cannot predict with good accuracy the changes produced when the fluid changes rapidly volume while passing from the injector to the clearance. This lack of accuracy in the model is attributed to the assumption of fully-developed velocity profile in the injection zone as well as to an isothermal behavior of the compressible fluid. CFD results shows that these effects are important and should not be neglected. A comparison of resulting forces (in the injection area) shows that the difference between the MRE and CFD models varies from 28% until 48% for a range of injection pressure from 4 to 8 bar and rotational velocity from 5000 to 20000 rpm. It is important to highlight that these relatively large discrepancies in the terms of resulting forces do not

take into account the hydrodynamic pressure outside of the injection zone. If such a hydrodynamic pressure is considered the discrepancies between MRE and CFD models are much smaller. That is the reason why the MRE results shows a relatively good agreement with the experimental results with an average error of 13.4% and standard deviation of 0.62 for the natural frequencies and an average error of 37.5% and 18.0 of standard deviation for the damping factor. It is possible to deduce that an important source of differences between theoretical model based on MRE and experimental results are the assumptions made on the injection. From the theoretical stability analysis for the flexible rotor supported by hybrid gas bearings one can conclude:

i) The use of a hybrid gas bearing improves the stability characteristic of the system.

ii) For a lower level of pressure the system becames more stable and also the damping increases, leading to the conclusion that an optimal value of injection pressure should exist.

iii) The injection in only two sides (horizontal) and an increase in bearing assymetric properties also increases the stability range.

## References

[1]     Vleugels P., Waumans T., Peirs J., Al-Bender F. & Reynaerts D. (2006) High-speed bearings for micro gas turbines: stability analysis of foil bearings. Journal of Micromechanics and Microengineering, 16 (9) 282–289.

[2]     Peng JP. & Carpino M. (1993) Calculation of Stiffness and Damping Coefficients for Elastically Supported Gas Foil Bearings, Transactions of the ASME 115, 20-27.

[3]     Hamrock B.J. (1994) Fundamentals in fluid film lubrication, McGraw-Hill, New York.

[4]     Cheng HS. & Trumpler PR. (1963) Stability of high-speed journal bearing under steady load. ASME J Eng Industry; 274–9.

[5]     Cheng HS. & Pan CHT. (1965) Stability analysis of gas-lubricated, self-acting, plain, cylindrical, journal bearings of finite length, using Galerkin's method. ASME J Basic Eng, 185–92.

[6]     Lund J.W. (1967) A theoretical analysis of whirl instability and pneumatic hammer for a rigid rotor in pressurized gas journal bearings. ASME J Lubri Tech, 154–65.

[7]     Lund J.W. (1968) Calculation of Stiffness and Damping Properties of Gas Bearings, Journal of Lubrication Technology, 90 (4) 793.

[8]     Wadhwa SS., Sinhasan R. & Singh DV. (1983) Analysis of orifice compensated externally pressurized gas bearings. Tribol Int;16, 203–11.

[9]     Han DC., Park SS., Kim WJ. & Kim JW. (1994) A study on the characteristics of externally pressurized air bearings. Precision Eng, 16, 164–73.

[10]    Zhang RQ. & Chang HS. (1995) A new type of hydrostatic/hydrodynamic gas journal bearing and its optimization for maximum stability. Tribol Trans, 38, 589–94.

[11]    Leonard R. & Rowe W.B. (1973) Dynamic force coefficients and the mechanism of instability in hydrostatic journal bearings. Wear; 23, 277–82.

[12]    Morosi S. & Santos I.F. (2011) On the modelling of hybrid aerostatic-gas journal bearings, Proceedings of the Institution of Mechanical Engineers, Part J: Journal of Engineering Tribology, 225 (7), 641–653.

[13]    Cerda Varela A., Nielsen B.B. & Santos I.F. (2013) Steady state characteristics of a tilting pad journal bearing with controllable lubrication: Comparison between theoretical and experimental results, Tribology International, 58, 85–97.

[14]    Lund J.W. & Thomsen K.K. (1978) A Calculation method and data for the dynamic coefficients of oil-lubricated journal bearings. In Topics in fluid film bearing and rotor bearing system design and optimization, 1–28.